LAWRENCE
LIVERMORE
NATIONAL
LABORATORY

UCRL-PROC-216720

MODELING NANOCRYSTALLINE GRAIN GROWTH DURING THE PULSED ELECTRODEPOSITION OF GOLD-COPPER

A. F. Jankowski

November 1, 2005

208th Meeting of the Electrochemical Society
Los Angeles, CA, United States
October 16, 2005 through October 21, 2005

MODELING NANOCRYSTALLINE GRAIN GROWTH DURING THE PULSED ELECTRODEPOSITION OF GOLD-COPPER

Alan F. Jankowski
Lawrence Livermore National Laboratory
7000 East Avenue, P.O. Box 808
Livermore CA 94550 USA

ABSTRACT

The process parameters of current density, pulse duration, and cell potential affect both the structure and composition of electrodeposits. The mechanism for nucleation and growth as determined from current transients yield relationships for nucleus density and nucleation rate. To develop an understanding of the role of the process parameters on grain size – as a design structural parameter to control strength for example, a formulation is presented to model the affects of the deposition energy on grain size and morphology. An activation energy for the deposition process is modeled that reveals different growth mechanisms, wherein nucleation and diffusion effects are each dominant as dependent upon pulse duration. A diffusion coefficient common for each of the pulsed growth modes demarcates an observed transition in growth from smooth to rough surfaces.

INTRODUCTION

The electrodeposition of nanocrystalline coatings often proceeds as a parametric study. That is, the process variables that can produce a refined grain size in the deposit are optimized by experimental iteration but, in general do not provide a clear causal basis from which to predict the grain size. There are numerous process variables that enable grain refinement as current density, pulse duration, and cell potential. These process parameters are codependent that in turn can affect the morphology of the coating and its surface. Thus, a means to understand the interrelationship between process variables and their influence on grain size is of importance to predictably enable the deposition of smooth and strong electrodeposits.

A recent experimental study (1) for the electrodeposition of nanocrystalline Au-Cu alloy coatings is briefly reviewed and compared with previous results (2-4). These results provide the test basis for assessing refinement of a new growth model (1). A formulation of the energy of the deposition process is presented that can quantitatively account for the resultant grain size of the electrodeposit as based on the cell potential (U), current density (j), and the forward pulse duration (t_p). These parameters enable a computation of the amount of energy (Q*) deposited in each pulse. This energy term is then related through an analogy of bulk diffusion to determine the grain size as based on ideal grain growth and the duration of each forward pulse. The activation energy (Q) for the growth process and an effective diffusion coefficient (D) can then be derived for the electrodeposition process.

SAMPLE PREPARATION

Coatings of gold-copper $Au_{(1-x)}$-$Cu_{(x)}$ (where 1< x <15 wt.%) are prepared through the aqueous process of pulsed plating metals from an ionic solution.(1) Averages of the current (i) and cell potential (U) are measured between a working cathode (sheet of titanium) and an inert platinum anode. These values are independently confirmed through Luggin capillary measurements using a standard Ag/AgCl reference electrode. A variation of a No. 2 Au bath is used as heated to a temperature of 55-75 °C with a pH of ~11 and per-liter volume constituents of 6.4-8.0 gm KCN, 6.4-8.8 gm $KCu(CN)_2$, and 1.0-3.0 gm $KAu(CN)_2$. It's generally accepted that electrodeposited gold from an alkaline cyanide solution proceeds through two mechanisms.(5-8) At lower cell potentials, i.e. the more positive potential, deposition proceeds by an adsorption of AuCN followed by the electron transfer. That is,

$$Au(CN)_2^- \rightarrow AuCN_{ads} + CN^-, \quad (1)$$

$$AuCN_{ads} + CN^- + 2H^+ + e^- \rightarrow Au + 2HCN. \quad (2)$$

At higher cell potential, i.e. the more negative potential, Au deposition occurs by direct charge-transfer between the gold complex in solution and the metal atom was found on reduction. In this case, the reaction proceeds as

$$Au(CN)_2^- + 2H^+ + e^- \rightarrow Au + 2HCN. \quad (3)$$

The adsorption of AuCN and the incorporation of impurities into Au deposits have an important affect on the nucleation and growth mechanism. The adsorption of AuCN is not likely influenced by the CN^- mass transfer when the concentration is high enough.

EXPERIMENTAL RESULTS

The Au-Cu foil composition is determined (1) by the atomic number–absorption–florescence (ZAF) semi-quantitative analysis procedure. The energy dispersive x-ray spectra of the electrodeposited foils reveal characteristic Cu *L* and Au *M* x-ray peaks that are used to quantify the composition. The surfaces of 10-30 μm thick foils are imaged using a scanning electron microscope. Surface morphologies, as seen in the Fig. 1 images

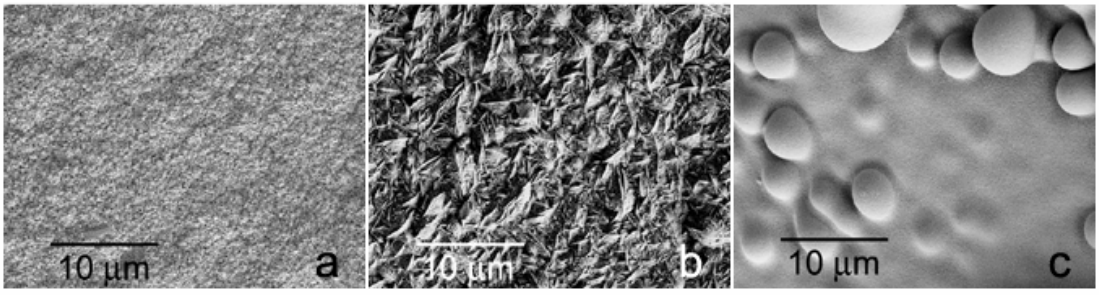

Figure 1. Scanning electron micrographs reveal the surface morphology of Au-5 wt.% Cu electrodeposits prepared using a current density of (a) 2 $mA \cdot cm^{-2}$, (b) 3 $mA \cdot cm^{-2}$, and (c) 5 $mA \cdot cm^{-2}$.

of Au-Cu coatings, vary with the process parameters from a smooth to a nodular growth. For example, in the Au-5 wt.% Cu deposits, the smooth features found in Fig. 1a at a small current density (j) of 2 $mA \cdot cm^{-2}$ can coarsen to the faceted-dendritic features of Fig. 1b with an increase in current density to 3 $mA \cdot cm^{-2}$, and further yet to nodular features at 5 $mA \cdot cm^{-2}$ as shown in Fig. 1c.

The as-deposited Au-5 wt.% Cu foils are found (1) to have an equiaxed nanocrystalline structure as revealed by transmission electron microscopy using bright-field imaging in plan view and selected-area diffraction. The crystallite size is quantified by analyzing peak-broadening of the Bragg reflections in the Fig. 2 Cu K_α x-ray diffraction scans taken in the $\theta/2\theta$ mode. There is no evidence for textured film growth in the diffraction scans. The polycrystalline pattern corresponds to the well-known disordered Au-Cu phase. The crystallite, i.e. grain, size (d_g) is determined from the (111) Bragg peak reflections and the Debye-Scherrer formulation as follows,

$$d_g = 0.9 \cdot \lambda \cdot (B \cdot \cos \Theta_B)^{-1} \qquad (4)$$

where λ is x-ray wavelength, and $2\Theta_B$ is the position of the Bragg reflection. The corrected full-width (B) at half-maximum intensity of the Bragg reflection is first determined by the formulation,

$$B^2 = B_m^2 - B_s^2 \qquad (5)$$

where B_m (in radians) is the full-width measured at half-maximum intensity, and B_s is 0.19° as measured for a Au (111) single-crystal.

The pulse duration and current density are generally known (9) to affect the grain size. A pulsed current can facilitate nuclei formation as the peak current density can be considerably higher than the limiting direct-current density. The x-ray diffraction results

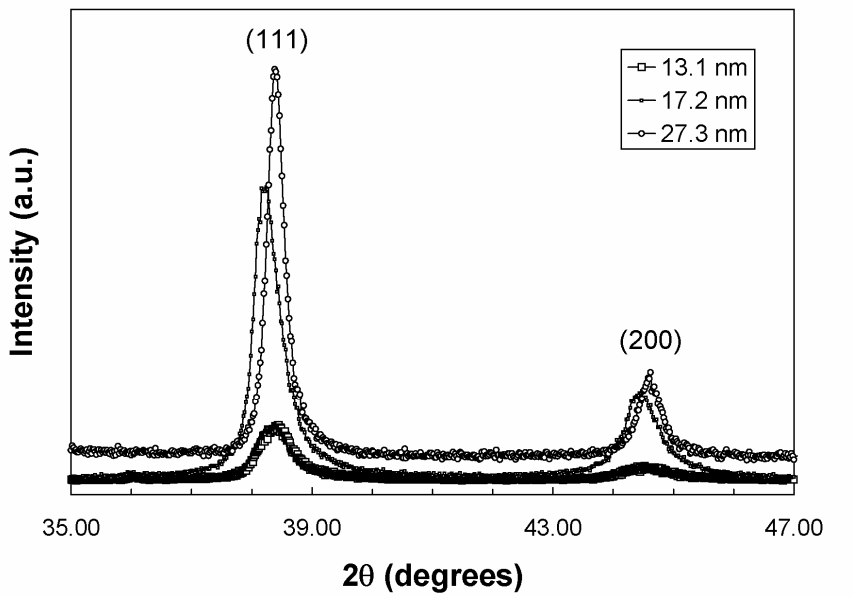

Figure 2. The x-ray diffraction scans reveal increased peak broadening consistent with the decrease in nanocrystalline grain size (d_g) for three equiaxed polycrystalline Au-5 wt.% Cu foils.

Table I. – Parameters of Au-Cu Deposition

short-pulse				long-pulse			
j (mA·cm^{-2})	$\mathbf{t_p}$ (ms)	**U** (Volts)	$\mathbf{d_g}$ (nm)	**j** (mA·cm^{-2})	$\mathbf{t_p}$ (ms)	**U** (Volts)	$\mathbf{d_g}$ (nm)
0.8	4	0.62	82.5	2.5	10	0.68	33.7
1.5	3	0.52	37.7	3.5	11.5	1.13	27.3
1.7	3	0.53	27.3	4.0	10	0.71	17.2
1.7	3	0.62	18.6	4.2	10	0.63	13.1
2.4	3	0.56	6.8	5.0	10	0.67	17.2
2.5	2	0.59	12.9	5.0	12	0.66	12.9
2.5	5	1.09	6.7	5.4	10	0.78	15.3
2.9	3	0.49	8.6	6.8	12	1.34	5.4
3.1	3	0.59	6.6	7.0	12	1.41	7.1
4.0	4	0.64	5.5	7.2	12	1.41	5.2
9.2	2	0.84	2.8	7.2	30	0.88	5.2
				7.2	30	0.88	4.2

for grain size along with the corresponding deposition parameters of current density and cell potential are listed in Table 1 with respect to the pulse duration. It's found (1) that the grain size decreases with an increase in the current density. There appears to be two growth regimes as distinguished based on the duration of the forward current pulse (t_p). The short pulse (t_p <5 msec) regime shows a faster decrease in d_g with increasing j than for the longer pulse (10< t_p <30 msec) regime. The relationship is best illustrated in Fig. 3

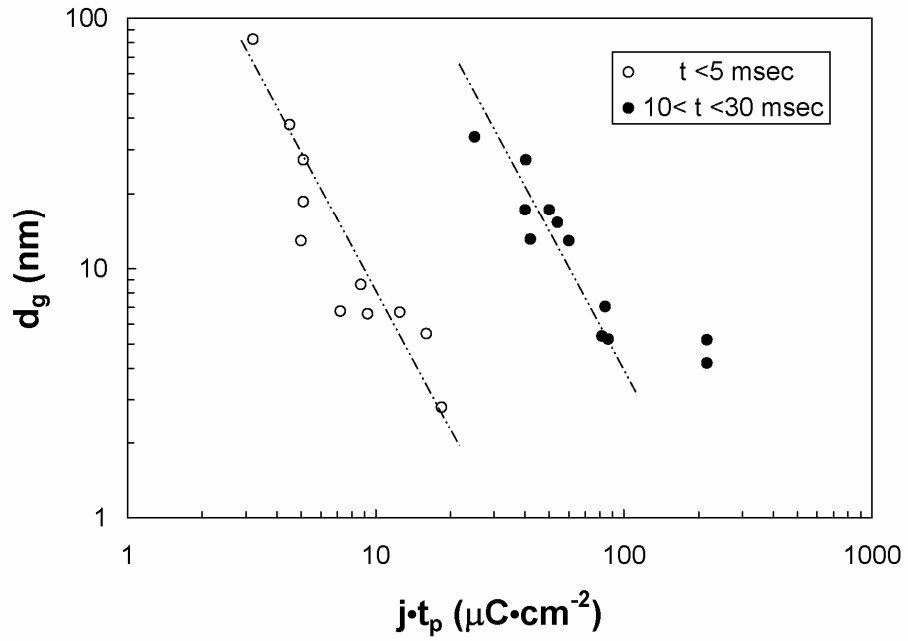

Figure 3. The average grain size d_g (nm), is plotted logarithmically as a function of the charge density, i.e. $j \cdot t_p$ ($\mu C \cdot cm^{-2}$), during each deposition pulse.

where the charge density during each deposition pulse ($j \cdot t_p$), as computed from Table 1, is plotted versus the grain size (d_g) using a logarithmic scale. Also, it is confirmed (1) that a decrease in the current density and cell potential favor the deposition of the more noble metal species (3-4) when depositing Au-Cu from cyanoalkaline-based solutions. These results seem to suggest a difference in the energetic barrier for stabilization of grain size between each pulse-duration mode. That is, the long pulse has an additional barrier to overcome that inhibits bulk-like diffusion whereas growth for the short pulse is primarily limited to overcoming the barriers for nucleation and perhaps surface diffusion as well. A difference in growth may then be apparent in the energetic barrier for grain formation. The long pulse mode should have an energy barrier for grain formation (Q_{lp}) that is greater than the energy for the short pulse mode (Q_{sp}). Both Q_{sp} and Q_{lp} should be less than the activation energy (Q_{tr}) obtained from high-temperature, tracer-diffusion studies.

GRAIN-GROWTH MODEL

A new grain growth model (1) is now developed with further detail where the determination of the activation energy (Q) for grain formation during electrodeposition provides the means to predict the size of nanocrystalline grain growth. The first premise is that a classic Arrhenius-type behavior for temperature-dependent diffusion in solids is assumed for the growth of electrodeposited coatings. That is, diffusion is mitigated by a negative exponential of the activation energy relative to the deposition energy. That is,

$$D = D_o \cdot e^{(-Q/Q^*)} \tag{6}$$

where the coefficient D can be defined by the standard expression for ideal grain growth (10), as

$$\partial(D) = \partial(d_g^{\,2} \cdot t_p^{\,-1}). \tag{7}$$

The activation energy (Q) in the exponent of eqn. (6) is divided by a term for the deposition energy (Q*) that corresponds to the driving force for grain formation. In the solid state Q* takes the form of $k_B \cdot T$ noting k_B is the Boltzmann constant and T is the absolute temperature.

The First Law of Electrochemistry, developed by Faraday in 1834, states that the chemical power of a current of electricity is in direct proportion to the absolute quantity of electricity which passes. In the Second Law of Electrochemistry, Faraday states that electrochemical equivalents coincide, and are the same, with ordinary chemical equivalents. Thus, from these principles, the mass of a substance produced at an electrode during electrolysis is proportional to the amount of electricity transferred at the electrode. Therefore, Q* is derived in an analogous manner as,

$$Q^* = \int^{n^* \cdot q^*} (U) \cdot dq \tag{8}$$

where U is electrical potential, and q is charge with the limit ($n^* \cdot q^*$) equal to the product of the unit charge (q*) per pulse with the unit number (n*) per pulse. That is, Q* is the energy of the charge per pulse and is defined in eqn. (8) as the integral product of the cell potential (U) with charge (q). Since the potential U equals $i \cdot R$, i.e. $(q \cdot t^{-1}) \cdot R$, an expression derived for Q* per mol with limit substitution for q is then,

$$Q^* = 0.5 \cdot N_A \cdot q^2 \cdot (t^{-1} \cdot R), \tag{9a}$$

$$Q^* = 0.5 \cdot N_A \cdot (n^* \cdot q^*)^2 \cdot (t^{-1} \cdot R), \tag{9b}$$

$$Q^* = 0.5 \cdot N_A \cdot (n^*)^2 \cdot q^* \cdot (q^* \cdot t^{-1} \cdot R), \tag{9c}$$

$$Q^* = 0.5 \cdot N_A \cdot (n^*)^2 \cdot q^* \cdot U^*, \tag{9d}$$

where N_A is the Avogadro number ($6.023 \cdot 10^{23}$ mol^{-1}) and U* then equals the product $(q^* \cdot t_p^{-1}) \cdot R$ as the average cell potential during the pulse cycle. The unit charge (q*) is equal to the product of the average current density (j) multiplied by the unit area (A*) and the duration of the pulse time (t_p). That is, an expression for q* readily follows as,

$$q^* = j \cdot A^* \cdot t_p. \tag{10}$$

An expression for the unit area (A*) with respect to the number (n_o) of atoms within an area projection (A_o) of a lattice cell is given as,

$$A^* = A_o \cdot (n_o)^{-1}. \tag{11}$$

where the projection area (A_o) is equivalent to the square of the average lattice parameter (a_o). Since there are singly charged ions in the electrodeposition of Au-Cu from the high-pH alkaline solution, it's assumed following the general expression of eqn. (3) that the number of ions (n*) equals the number of atoms (n_o). For a face-centered-cubic lattice of Au-Cu, n_o equals two, hence eqn. (9d) can be rewritten using eqns. (10) and (11) as

$$Q^* = 0.5 \cdot N_A \cdot (n_o)^2 \cdot (j \cdot A^* \cdot t_p) \cdot U^*, \tag{12a}$$

$$Q^* = 0.5 \cdot N_A \cdot (n_o)^2 \cdot j \cdot (A_o \cdot n_o^{-1}) \cdot t_p \cdot U^*, \tag{12b}$$

$$Q^* = (0.5 \cdot n_o) \cdot N_A \cdot j \cdot (a_o^2) \cdot t_p \cdot U^*, \tag{12c}$$

$$Q^* = N_A \cdot (j \cdot t_p \cdot a_o^2) \cdot U^*, \tag{12d}$$

Following eqns. (6), (7), and (12) – a plot of $(Q^*)^{-1}$ with $\ln[\partial(d_g^2 \cdot t_p^{-1})]$ as shown in Fig. 4 should yield a straight line, the slope of which is equivalent to -Q. The value for Q* is computed using eqn. (12) with the Table 1 data and a value for a_o equal to 0.408 nm as determined from the average position of the Bragg reflections seen in Fig. 2. Note that U has a negative sign in the Fig. 4 plot following eqn. (3). The short-pulse (t_p <5 msec) and long-pulse (10< t_p <30 msec) results obtained for the grain size measurements were plotted in Fig. 3. Two straight lines can be drawn in Fig. 4 corresponding to eqn. (6) yielding an activation energy (Q) for grain formation in the long-pulse mode (Q_{lp}) equal to 146 $kJ \cdot mol^{-1}$ (i.e. 1.52 $eV \cdot atom^{-1}$) and in the short-pulse mode (Q_{sp}) equal to 15.2 $kJ \cdot mol^{-1}$ (i.e. 0.16 $eV \cdot atom^{-1}$) with a D_o value of 4×10^{-12} $cm^2 \cdot sec^{-1}$. As was first seen in the Fig. 3 logarithmic plot of grain size variation with charge density, there are two regimes for nanocrystalline growth – a short and long pulse mode, each with a distinctly different activation energy. For comparison, an activation energy (Q_{tr}) for grain growth of 1.85 $eV \cdot atom^{-1}$ is reported (11-12) for high-temperature tracer diffusion studies of Au^{198} in both Au and Cu. As anticipated, $Q_{sp} < Q_{lp} < Q_{tr}$.

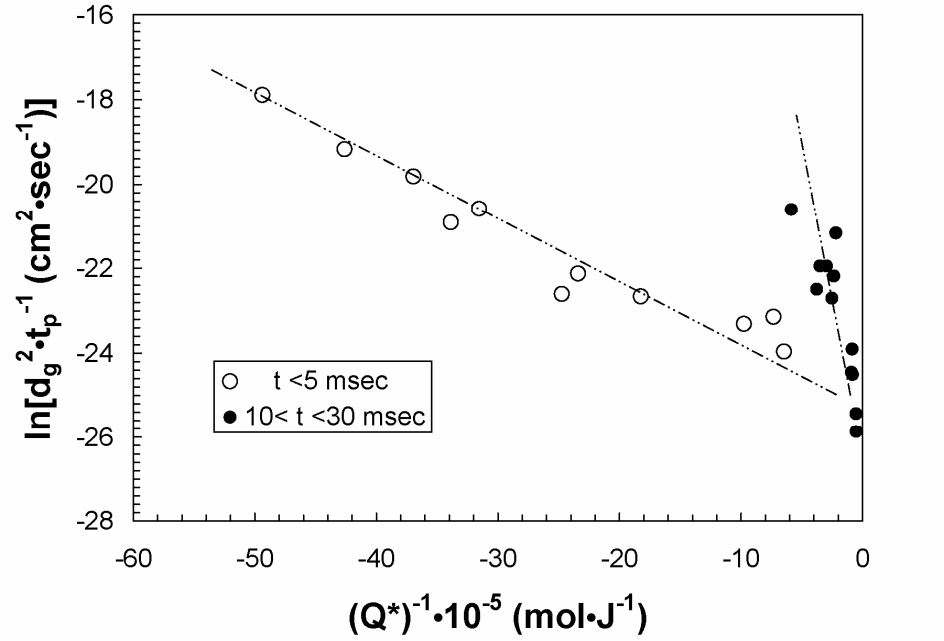

Figure 4. The natural logarithm of grain size d_g squared (cm^2), divided by the pulse duration t_p (sec^{-1}) yields an Arrhenius plot with the inverse of deposition energy Q* ($mol \cdot J^{-1}$).

DISCUSSION

To form a nanocrystalline electrodeposited foil, the concept (9, 13) taken is to promote massive nucleation with reduced grain growth. The individual curves shown in Fig. 3 confirm this concept. An increase in pulsed charge density ($j \cdot t_p$) at constant t_p favors a reduced grain size (d_g). This result indicates that the number of nucleation sites increases with charge density. The parallel offset between the linear curves suggests that this concept scales with pulse duration. Similarly, at constant pulsed-charge density, the vertical separation between the parallel curves indicates that a shorter on-pulse favors a refinement in grain size as expected.

The nanocrystalline grain size can be metastable as annealing above 423 K is shown (14) to yield exothermic reactions in differential scanning calorimetry traces that are associated with both grain growth and ordering of the Au-Cu alloy. Also, the refinement of grain size to the nanoscale is shown (1, 9, 15-18) to enhance the microhardness of electrodeposits in accordance with Hall-Petch type behavior.

The various growth morphologies that appear in electrodeposits can be directly related to the electrolyte, additives, and the concurrent deposition process. For example, star-shaped Au crystallites are reported (19) using a citrate bath of $KAu(CN)_2$ containing an additive of benzyl di-methyl phenyl ammonium chloride. The additive will cause an electrochemical depolarization of the process resulting in a preferred (110) texture of crystallites with multiple twinning giving rise to a pentagonal symmetry. The growth of nanocrystalline Au-Cu electrodeposits can start with a Au-rich region that changes in concentration with increasing thickness (14) to equilibrate at an alloy composition. Often, the Au-Cu deposits can have a microstructure of rounded crystal colonies (as seen in Fig.

1c) that are each several microns in size – a result of several nucleation events. Porosity can then occur at triple junctions. The results for the Au-Cu surfaces shown in Fig. 1 infer that there is a range of current density and pulse to produce a smooth surface. Typical results (1) for Au-Cu electrodeposits evidence smooth surfaces at a low current density of 0.8-4 $mA \cdot cm^{-2}$, a short-to-intermediate pulse length of 2-12 msec, and a low cell potential of 0.53-0.71 V. These findings are consistent with other reports (20) wherein a current density less than 4 $mA \cdot cm^{-2}$ and a reaction potential of 0.6 V for alkaline solutions with a pH value greater than 9-to-10 are shown to produce smoother foils with a minimum of residual stress. With reference to the Fig. 4 plot, there appears to be a range of diffusion available in either the short-pulse or long-pulse mode to produce a smooth Au-Cu surface as shown in Fig. 1a. A smooth surface results when ln(D), i.e. $\ln[\partial(d_g^2 \cdot t_p^{-1})]$, is greater than -22.0 for either the short- or long-pulse mode. The surface features roughen and become nodular as ln(D) decreases from -22 to -26.

SUMMARY

Empirical relationships are developed that relate the time-averaged deposition process parameters of current density (j), on-time pulse duration (t_p), and cell potential (U) to the growth morphology and nanocrystalline grain size. Regimes for nanocrystalline growth include a short-pulse and long-pulse mode, each with a distinct activation energy Q*. For deposition from high-pH cyanoalkaline-based solutions, a mathematical derivation reveals that Q* can be equated to the product $N_A \cdot (j \cdot t_p \cdot a_o^2) \cdot U$ where a_o is the lattice parameter and N_A is Avogadro's number. The long-pulse mode with a Q_{lp}* of 1.52 $eV \cdot atom^{-1}$ has the additional contribution of bulk-like diffusion whereas the short-pulse mode with a Q_{sp}* of 0.16 $eV \cdot atom^{-1}$ is primarily limited to nucleation with perhaps some surface diffusion. For either pulse condition, a transition from a rough (or nodular) growth to a smooth surface results with an increase in the kinetics of diffusion, that is when ln(D) is less negative than a value of -22.

ACKNOWLEDGEMENTS

This work was performed under the auspices of the U. S. Department of Energy by the University of California, Lawrence Livermore National Laboratory under Contract No. W-7405-Eng-48.

REFERENCES

1. A.F. Jankowski, C.K. Saw, J.F. Harper, R.F. Vallier, J.L. Ferreira, J.P. Hayes, University of California, Lawrence Livermore National Laboratory, Livermore, CA, UCRL-JRNL-210132, *Thin Solid Films*, in press (2005)
2. J.W. Dini, *Electrodeposition: the materials science of coatings and substrates*, Noyes Publications, Park Ridge, NJ (1993)
3. B. Bozzini, G. Giovannelli, and P. Cavallotti, *J. Appl. Electrochem.*, **29**, 685 (1999)
4. B. Bozzini and P.L. Cavallotti, *J. Electrochem. Soc.*, **148**, C231 (2001)
5. D.M. MacArthur, *J. Electrochem. Soc.*, **119**, 672 (1972)
6. E.T. Eisenmann, *J. Electrochem. Soc.*, **119**, 717 (1972)

7. M. Beltowska-Brezezinska, E. Dutkiewicz, and W. Lawicki, *J. Electroanal. Chem.*, **99**, 341 (1979)
8. P. Bindra, D. Light, P. Freudenthal and D. Smith, *J. Electrochem. Soc.*, **136**, 3616 (1989)
9. U. Erb, G. Palumbo, R. Zugic, K.T. Aust, in *Processing and Properties of Nanocrystalline Materials*, C. Suryanarayana, J. Singh, F.H. Froes, Editors, p. 93, The Minerals, Metals and Materials Society, Warrendale, PA (1996)
10. R.E. Reed-Hill, *Physical Metallurgy Principles*, pp. 304-310, Van Nostrand, New York, NY (1973)
11. A. Chatterjee and D.J. Fabian, *Acta Metallurgica*, **17**, 1141 (1969)
12. H.M. Gilder and D. Lazarus, *J. Phys. Chem. Solids*, **26**, 2081 (1965)
13. R.T.C. Choo, J.M. Toguri, A.M. El-Sherik, and U. Erb, *J. Appl. Electrochem.*, **25**, 384 (1995)
14. L. Battezzati, M. Baricco, M. Belotti, and V. Brunella, *Mater. Sci. Forum*, **360-362**, 253 (2001)
15. R.W. Siegel, *Mater. Sci. Forum*, **235-238**, 851 (1997)
16. Y. Lu and P.K. Liaw, *J Metals*, **53 (3)**, 31 (2001)
17. J. Schiotz, F. Di Tolla, and K. Jacobsen, *Nature*, **391**, 561 (1998)
18. F. Dalla Torre, H. Van Swygenhoven, and M. Victoria, *Acta Materialia*, **50**, 3957 (2002)
19. B. Bozzini, A. Faningliulo, and M. Serra, *J. Crystal Growth*, **231**, 589 (2001)
20. P.A. Kohl, in *Fundamentals of Electrochemical Deposition*, M. Paunovic and M. Schlesinger, Editors, John Wiley Publishers, New York, NY (1999)